Published in final edited form as:
Biochemistry. 2011 September 20; 50(37): 7868–7880. doi:10.1021/bi200753b.

Self-assembly of *E. coli* MutL and its complexes with DNA

Anita Niedziela-Majka[$], **Nasib K. Maluf**[#], **Edwin Antony**, and **Timothy M. Lohman**[*]
Department of Biochemistry and Molecular Biophysics, Washington University School of Medicine, 660 S. Euclid Avenue, Box 8231, St. Louis, MO 63110-1093 USA

Abstract

The *E. coli* MutL protein regulates the activity of several enzymes, including MutS, MutH and UvrD, during methyl-directed mismatch repair (MMR) of DNA. We have investigated the self association properties of MutL and its binding to DNA using analytical sedimentation velocity and equilibrium. Self association of MutL is quite sensitive to solution conditions. At 25°C in Tris at pH 8.3 MutL assembles into a heterogeneous mixture of large multimers. In the presence of potassium phosphate at pH 7.4, MutL forms primarily stable dimers, with the higher order assembly states suppressed. The weight averaged sedimentation coefficient of MutL dimer in this buffer is equal to $\overline{s}_{20,w}$ = 5.20 ± 0.08, suggesting a highly asymmetric dimer (f/f_o = 1.58 ± 0.02). Upon binding the non-hydrolyzable ATP analogue, AMPPNP/Mg^{2+}, the MutL dimer becomes more compact ($\overline{s}_{20,w}$ = 5.71 ± 0.08 S, f/f_o = 1.45 ± 0.02), probably reflecting reorganization of the N-terminal ATPase domains. A MutL dimer binds to an 18 bp duplex with a 3'-(dT_{20}) single stranded flanking region, with apparent affinity in the micromolar range. AMPPNP binding to MutL increases its affinity for DNA by a factor of ~10. These results indicate that the presence of phosphate minimizes further MutL oligomerization beyond a dimer and that differences in solution conditions likely explain apparent discrepancies in previous studies of MutL assembly.

Keywords

DNA repair; self-association; protein-DNA interaction; analytical ultracentrifugation

In *E. coli*, DNA replication errors are primarily corrected by the methyl-directed mismatch repair (MMR) pathway (1). The MutL protein plays a central role in this process by regulating a number of events from mismatch recognition to DNA duplex unwinding (2–4). MMR begins with recognition of the aberrant base pair by a MutS dimer in a process requiring ATP (5). Subsequently, MutL, in an ATP bound form, interacts with the MutS - DNA complex (6) (7) (2), which activates a latent endonuclease associated with MutH. MutH then introduces a nick into the unmethylated (newly replicated) DNA strand at the nearest hemi-methylated d(GATC) site, which can be positioned on either side of the mismatch (8). The mechanistic details of this process are not fully understood, although models have proposed either looping of the intervening DNA or converting MutS into a sliding clamp which can then search for the nearest hemi-methylated site (9–12). In the next step MutL recruits the UvrD protein, a 3' to 5' superfamily 1 (SF 1) DNA helicase (13–15),

[*]Address correspondence to: T. M. Lohman, Department of Biochemistry and Molecular Biophysics, Washington University School of Medicine, 660 S. Euclid, St. Louis, MO 63110, 314-362-4393, FAX: 314-362-7183, lohman@biochem.wustl.edu.
[#]Current address: Department of Pharmaceutical Sciences, UCHSC, School of Pharmacy, Denver, CO 80262
[$]Current address: Gilead Sciences, Inc., 333 Lakeside Dr., Foster City, CA 94404

Supporting information available
Supplemental Figure 1, Supplemental Table 1 summarizing all the sedimentation coefficients measured in this study, and Supplemental Table 2 summarizing all the binding constants for AMPPNP and DNA binding to MutL are included. This material is available free of charge via the Internet at http://pubs.acs.org.

to the nicked DNA substrate. In MMR, UvrD initiates DNA unwinding from the nick and proceeds past the mismatch, which can be as long as 1–2 kilobase pairs in length (16). The unwound nascent DNA strand is digested by cellular exonucleases (17, 18), resulting in a gap which is then filled in by DNA polymerase III, with the final nick sealed by DNA ligase (19).

The mechanism by which MutL stimulates the UvrD helicase, which by itself has a rather low unwinding processivity (20), to unwind longer stretches of DNA is not fully understood (21). It has been shown that MutL increases the unwinding activity of UvrD *in vitro* more than an order of magnitude under multiple turnover conditions (22) and that the C-terminus of MutL interacts with the N- and C- termini of UvrD (23).

MutL possesses a weak ATPase activity which is essential for MMR and which is further stimulated around five-fold by ssDNA binding (6, 24, 25). Moreover, ATP binding by MutL, but not hydrolysis, is required to stimulate the activity of UvrD (6). Based on these observations, a model was proposed in which MutL functions by continually loading multiple UvrD helicases onto a DNA substrate, thus facilitating unwinding of long stretches of DNA (21, 26). It was also suggested that MutL loads UvrD onto the appropriate DNA strand to ensure that unwinding will proceed in the direction of the mismatch (21, 26). This would prevent bi-directional DNA unwinding from the nick, as was observed *in vitro* in the absence of MutL (15, 27).

UvrD self-associates into dimers and tetramers *in vitro* (28). Furthermore, pre-steady state kinetic experiments demonstrated that the UvrD dimer possesses helicase activity (29–33). Although a UvrD monomer is capable of translocating along ss DNA with 3’ to 5’ directionality and high processivity, a monomer does not unwind DNA processively *in vitro* (34–36). Therefore, a plausible mechanism to explain the stimulation of the helicase activity of UvrD by MutL could be that MutL stabilizes the UvrD dimer (or a higher order oligomer). Alternatively, MutL may activate the helicase activity of the UvrD monomer. This could be accomplished by relieving the auto-inhibition function of the 2B sub-domain of UvrD. Such auto-inhibitory activity of the 2B sub-domain was unequivocally demonstrated for the Rep helicase (37).

Crystal structures are available for both the N- and C- terminal regions of the *E. coli* MutL protein. The C-terminal 20 kDa region of MutL crystallizes as a dimer (7), whereas the N-terminal 40 kDa ATPase domain of MutL crystallizes as a monomer in the absence of nucleotide, but a dimer is observed in the presence of a non-hydrolyzable ATP analogue, with one AMPPNP bound per subunit. In this structure part of the protein-protein interface as well as the lid of the ATP binding pocket, are created upon folding of ~ 60 amino acid residues surrounding the nucleotide binding site (24, 38).

Based on glycerol gradient centrifugation and gel filtration chromatography (3°C, 50 mM potassium phosphate, pH 7.4, 50 mM KCl, 0.1 mM EDTA, 1 mM DTT), MutL was reported to be an elongated dimer (39). The dimensions of the MutL dimer calculated from light scattering experiments (24°C, 20 mM Tris, pH 8.0, 200 mM KCl, 5 mM $MgCl_2$, 1 mM DTT, 0.1 mM EDTA) (7) differ substantially from the values obtained in the gel filtration experiments. Both sets of experiments were performed in different buffer and temperature conditions and the effect of [MutL] on the assembly state of MutL was not examined systematically.

MutL seems to be a very versatile macromolecule: it interacts with and regulates activities of many proteins participating in MMR (1) (21). In order to decipher the molecular mechanism of this regulation and to understand how MutL stimulates UvrD helicase activity it is necessary to understand the self-assembly properties of MutL and its interaction with

DNA. Towards this end, we have examined the self-association properties of MutL over a range of solution conditions using both sedimentation equilibrium and velocity methods, as well as its interaction with an 18 bp DNA duplex possessing a 3'-dT_{20} tail (3'(dT_{20})ds18).

Materials and Methods

Buffers

Buffers were made with reagent grade chemicals and distilled water that was further deionized by treatment with a Milli-Q water purification system (Millipore Corp., Bedford, MA). Spectrophotometric grade glycerol was from Aldrich (Milwaukee, WI). Buffer K is 24.3 mM KH_2PO_4, 5.7 mM K_2HPO_4, 50 mM KCl, 2 mM 2-mercapthoethanol, 0.2 mM PMSF (pH 7.4 at 25°C). For the composition of all others buffers see Table 1. Stock solutions of AMPPNP (5'-adenylylimidodiphosphate lithium) (Sigma-Aldrich, St. Louis, MO) were prepared in Milli-Q H_2O, neutralized to pH 7.5 by titration with NaOH and stored in 10 µl aliquots at −20°C. AMPPNP concentration was determined spectrophotometrically using an extinction coefficient of 15.4×10^3 $M^{-1}cm^{-1}$ at 259 nm.

MutL expression and purification

MutL was expressed and purified to greater than 98% homogeneity as described (39), but with the following modifications. BL21(DE3)pLysS cells were freshly transformed with the MutL expression plasmid L1-pET3a, kindly provided by Paul Modrich (Duke University Medical Center, Durham, NC). Cells were grown at 37°C in 4 liters of LB broth (40) supplemented with 1 % glucose (w/v), 4 µg/ml thymine, 10 µg/ml thiamine, 10 mM potassium phosphate (pH 7.4 at 25°C), 100 µg/ml ampicillin and 35 µg/ml chloramphenicol. MutL expression was induced at (OD_{600} = 1.0) with 1mM IPTG for 3.5 hours. All purification steps were performed at 4°C. 25g of cells were resuspended in ice cold buffer containing 50 mM potassium phosphate, 1 mM EDTA, 2 mM 2-mercapthoethanol, 0.2 mM PMSF (pH 7.4 at 25°C) using 7 ml of buffer per 1 gram of paste. Suspension was incubated on ice for 30 min to allow disruption of bacterial cell walls by lysozyme expressed from the plasmid pLysS, followed by 30 min incubation with 0.05 % (w/v) sodium deoxycholate. Viscosity of the lysate was reduced by sonication on ice for 2 to 5 minutes using 15–30 s bursts at 50% duty and power setting of 7 (Model W225, Heat System - Ultrasonics, Inc., Farmingdale, NY). Streptomycin sulfate and ammonium sulfate precipitation was performed as described (39). Ammonium sulfate pellet was dissolved in 200 ml of buffer K and the resulting solution was clarified by centrifugation at 13,000 rpm for 45 min and divided into two 100 ml pools which were purified sequentially on ceramic hydroxyapatite column (CHT type I, Bio-Rad, Hercules, CA). Protein solution (100 ml) was loaded (10 ml/min) onto ceramic hydroxyapatite resin (50 mL) equilibrated with buffer K while mixing with buffer K such that the conductivity was no higher than that of buffer K containing 75 mM potassium phosphate. Hydroxyapatite chromatography was performed as described (39). Fractions containing MutL were pooled and loaded onto a Poros 50 HS strong cation exchange column (50 mL) (Applied Biosystems, Forester City, CA) equilibrated with buffer K. The column was loaded (10 ml/min) while mixing the protein solution with buffer containing 30 mM potassium phosphate, 2 mM 2-mercapthoethanol, 0.2 mM PMSF (pH 7.4 at 25°C) in order to reduce the KCl concentration to 75 mM. The column was washed with buffer K (200 mL) and eluted with a 500 mL linear gradient of KCl (50 – 400 mM) in 30 mM potassium phosphate, 2 mM 2-mercaptoethanol, 0.2 mM PMSF (pH 7.4 at 25°C). MutL elutes at 300–350 mM KCl. Fractions containing MutL were pooled and dialyzed overnight vs. buffer K. After clarification by centrifugation at 13,000 rpm for 45 min the protein was loaded (2 mL/min) onto a ssDNA cellulose column (50 mL) equilibrated with buffer K and washed with buffer K (200 mL) and then buffer (300 mL) containing 30 mM potassium phosphate, 100 mM KCl, 2 mM 2-mercapthoethanol, 0.2 mM PMSF (pH 7.4 at 25°C).

MutL was eluted with 30 mM potassium phosphate, 250 mM KCl, 2 mM 2-mercapthoethanol, 0.2 mM PMSF (pH 7.4 at 25°C) and pooled fractions were dialyzed vs. storage buffer (buffer M). MutL aliquots in buffer M were flash frozen in liquid nitrogen and stored at − 80°C (5 – 6 μM monomer).

Prior to use in the experiments MutL protein was thawed at 10°C in ice/water bath, centrifuged at 14,000 rpm for 15 min at 4°C and dialyzed extensively into the appropriate buffer at 4°C. The extinction coefficient of MutL monomer in buffer M20/20 (ε_{280} = 50172 ± 1204 $M^{-1}cm^{-1}$) was determined experimentally as described (41).

DNA

Oligodeoxynucleotides were synthesized using an ABI model 391 DNA synthesizer (Applied Biosystems, Foster City, CA) and purified as described (42, 43). The DNA used in this study (3'ss$(dT)_{20}$ds18-Cy3) consisted of an 18 bp duplex with a 3' $(dT)_{20}$ single stranded tail and labeled with a Cy3 fluorophore at the 5' end of the strand with 3'ssDNA tail. The sequence of the strand without the 3' ssDNA tail was 5'-GCCTCGCTGCCGTCGCCA-3'. Oligodeoxynucleotides were dialyzed into 10 mM Tris-HCl (pH 8.3) and stored at −20°C and the concentration was determined spectrophotometrically as described (44) using an extinction coefficient of 5000 $M^{-1}cm^{-1}$ for Cy3 at 260 nm and 150000 $M^{-1}cm^{-1}$ at 550 nm (Glenn Research, Sterling, VA). The duplex DNA was created by mixing a 1:1 molar ratio of the two strands in 10 mM Tris-HCl, 50 mM NaCl (pH 8.3 at 25°C), heating to 95°C for 5 minutes and then cooling to room temperature over a period of 2 hours. Duplex formation was confirmed by native PAGE on 10% acrylamide gel. DNA was dialyzed vs. the appropriate buffer using 8,000 Da molecular weight cut-off dialysis tubing (Spectrum Medical Industries, Inc., Houston, TX). The concentration of 3'ss$(dT)_{20}$ds18-Cy3 DNA in buffer M20/20 was determined spectrophotometrically using ε_{550} = 126311 ± 2114 $M^{-1}cm^{-1}$ at 550 nm (ε_{260} = 460563 ± 9011 $M^{-1}cm^{-1}$ and ε_{280} = 277722 ± 6953 $M^{-1}cm^{-1}$)(28).

Analytical Ultracentrifugation

Dialyzed protein and DNA samples were filtered (0.22 μm centrifugal filter devices, Ultrafree-MC, Millipore Corp., Bedford, MA) by centrifugation at 6,000 rpm for 5 min at 4°C. Sedimentation equilibrium and velocity experiments were performed using ProteomeLab XL-A analytical ultracentrifuge equipped with An50Ti rotor (Beckman Coulter, Fullerton, CA) at temperatures of 5°C or 25°C. Absorbance data for MutL in the absence of DNA and AMPPNP were collected by scanning the sample cells at wavelengths of either 230 nm or 280 nm depending on [MutL]. In experiments performed with AMPPNP, nucleotide at the same final concentration was placed in the reference channel of the centerpiece. Experiments performed with 35 μM AMPPNP were scanned at 230 nm or 280 nm. The contribution from the absorbance of 35 μM AMPPNP at the highest MutL concentration used (3.78 μM MutL monomer) was 27 % and 7 % at 280 nm and 230 nm, respectively. For experiments performed with increasing [AMPPNP], the cells were scanned at 292 nm where the absorbance of nucleotide cofactor is minimal. Experiments performed with Cy3-labelled DNA were scanned at 550 nm. There was no absorbance change accompanying MutL binding to 3'ss$(dT)_{20}$ds18-Cy3 duplex DNA (28).

For sedimentation equilibrium, samples (120 μl) were loaded into the three channels of an Epon charcoal-filled six-channel centerpiece with 122 μl of buffer in the reference chambers. Absorbance data were collected by scanning the sample cells at wavelength at intervals of 0.001 cm in the step mode with seven averages per step. Each experiment was conducted at three to four rotor speeds, starting with the lowest and finishing with the highest rotor speed. At each speed samples were sedimented until they reached equilibrium

(defined as successive superimposable scans taken 2 hours apart). Sedimentation equilibrium data were edited using program REEDIT (Jeff Lary, National Analytical Ultracentrifugation Center, Storrs, CT) in order to extract the data between the sample meniscus and the bottom of the cell chamber. The resulting concentration profiles were fitted to a sum of exponential terms (Eq. 1) using a nonlinear least-squares (NLLS)

$$A_T = \sum_{i=1}^{n} \exp(\ln A_{0,i} + \sigma_i (r^2 + r_{ref}^2)/2) + b \quad (1)$$

routine,were A_T is the total absorbance at radial position r; $A_{0,i}$ is the absorbance of component i at the reference position (r_{ref}); b is baseline offset; $\sigma_i = [M_i (1 - \bar{\upsilon}_i \rho)\omega^2]/RT$, is the reduced molecular mass of component i, where M_i is the molecular mass; $\bar{\upsilon}_i$ is the partial specific volume; ρ is buffer density; ω is an angular velocity of the rotor, T is absolute temperature, and R is the gas constant. ρ was calculated from buffer composition using the software Sedenterp (45). The NLLS fitting program WinNonlin (46) was used for analysis of concentration profiles obtained for a system with a single species (n = 1 in Eq. 1), whereas data for a multi component system (n > 1 in Eq. 1) were fitted with Scientist (Micromath Scientific Software, St. Louis, MO). Global NLLS fit of the absorbance profiles to Eq. 1 returns M for each component. For MutL at 25°C, $\bar{\upsilon}$ = 0.7414 ml/g as calculated from amino acid composition according to Eq. 2 (47)) as implemented in Sedenterp (45), where n_i is the number of amino acids of type i.

$$\bar{\upsilon} = \left(\sum_{i=1}^{n} n_i M_i \bar{\upsilon}_i \right) / \left(\sum_{i=1}^{n} n_i M_i \right) \quad (2)$$

Partial specific volumes at temperature, T were calculated from $\bar{\upsilon}_T = \bar{\upsilon}_{25} + 4.25E^{-4}(T - 25)$ (48). The partial specific volume for 3'ss$(dT)_{20}$ds18-Cy3 duplex DNA was obtained experimentally by analyzing sedimentation equilibrium experiments at three different loading concentrations (1.2 μM, 2 μM and 4 μM) and four rotor speeds (18,000; 22,000; 27,000 and 33,000 rpm) at 25°C in buffer M20/20. Absorbance data were collected at 550 nm and twelve concentration profiles were fitted globally by NLLS methods with WinNonlin (46) using a single ideal species model (n =1 in Eq. 1). From the best fit value of the reduced molecular mass, a value of $\bar{\upsilon}_{DNA}$ = 0.5871 ± 0.0178 ml/g at 25°C was calculated, assuming a molar mass calculated from the DNA composition ($M_{Cy3\text{-}DNA}$ = 17,594.79 g/mol). The weight average $\bar{\upsilon}$ for the $MutL_2$-DNA complex ($\bar{\upsilon}_{MutL2\text{-}DNA}$ = 0.7237 ± 0.002 ml/g) and $MutL_2$ bound to AMPPNP in the absence ($\bar{\upsilon}_{MutL2\text{-}AMPPNP}$ = 0.7392 ml/g) and presence of DNA ($\bar{\upsilon}_{MutL2\text{-}DNA\text{-}AMPPNP2}$ = 0.7219 ± 0.002 ml/g) at 25°C were calculated from $\bar{\upsilon}$ and molar masses of the individual components (M_{MutL2} = 135,847.9 g/mol, M_{AMPPNP} = 506.2. g/mol) according to Eq. 2 (47) (using $\bar{\upsilon}_{ATP}$ = 0.4421 ml/g). Buoyant molecular weight of the complex can be calculated from the molar mass and the weight averaged partial specific volume of the complex, with equation: $M_b = M(1 - \bar{\upsilon}\rho)$.

In sedimentation velocity experiments the sample (380 μl) and buffer (392 μl) were loaded into each sector of an Epon charcoal-filled 2-sector centerpiece. Experiments were performed at 25°C or 5°C at 42,000 rpm. Absorbance data were collected every 2.5 min by scanning at the selected wavelength (230 nm, 280 nm, 292 nm or 550 nm) at intervals of 0.003 cm with one average in a continuous scan mode. The continuous sedimentation coefficient distribution, c(s), was calculated using SEDFIT (49, 50). The molar mass of the macromolecule can be estimated from the best fitted values of a sedimentation (s) and diffusion (D) coefficients according to equation (Eq. 3) (51).

$$M=sRT/[D(1-\bar{\upsilon}\rho)] \quad (3)$$

Calculated *s* values were converted to $s_{20,w}$ using Sedenterp (45). Buffer density and viscosity were calculated from buffer composition using the tabulated values in Sedenterp (45). Weight average sedimentation coefficients ($\bar{s}_{20,w}$) were calculated by integration of the area under the c(s) curves (52). The frictional coefficient ratio, (f/f_o), where f is the frictional coefficient of the macromolecule and f_o is the frictional coefficient of a hydrated sphere of equivalent mass was calculated using eq. (4),

$$\frac{f}{fo}=\left(\frac{M^2(1-\bar{\upsilon}\rho)^3}{162\pi^2(s_{20,w})^3\eta^3N_A^2\left(\bar{\upsilon}+\delta\upsilon^0_{H\,2O}\right)}\right)^{1/3} \quad (4)$$

where η, ρ, $\upsilon^0_{H\,2O}$ are the viscosity, density and partial specific volume of pure water at 20°C, respectively, N_A is Avogadro's number, δ is the macromolecule hydration in grams of water bound per gram of macromolecule (53, 54). An estimated value of the degree of hydration for MutL equal to δ = 0.2806 g of water bound per gram of protein was used, based on the amino acid sequence of MutL and the method of Kuntz (55) as implemented in Sedenterp and applying the correction of Lin *et al*. (56), which takes into account that only around 70 % of the water molecules calculated by Kuntz's method seems to be associated with folded proteins. For 3'(dT_{20})-ds18-Cy3 DNA a value of δ = 0.497 g of water bound per gram of DNA was used. This value was calculated based on weight average contribution of single stranded and double stranded regions in DNA molecule and published values of δ_{dsDNA} = 0.55 and δ_{ssDNA} = 0.40 g of water bound per gram of DNA (57, 58). For a MutL dimer bound to 3'(dT20)-ds18-Cy3 DNA a value of δ = 0.305 g of water bound per g of protein-DNA complex was used to calculate the weight average of hydration of MutL dimer and hydration of the DNA molecule.

Analysis of AMPPNP and DNA binding to MutL

For AMPPNP binding to a MutL dimer (total concentration of MutL dimer, $[M_{2,T}]$ = 1.75 μM), the dependence of the weight average sedimentation coefficient ($\bar{s}_{20,w}$) on total [AMPPNP] ($[X_T]$) was analyzed assuming two identical and independent binding nucleotide binding sites per MutL dimer, returning a step-wise microscopic association constant (k). Data were fitted to equation (5) using a Scientist program (Micromath, St.

$$\bar{s}_{20,w}=\frac{C*2*k*[X_f]+D}{1+k[X_f]} \quad (5)$$

Louis, MO), where C and D are the $\bar{s}_{20,w}$ for fully saturated and AMPPNP free MutL dimer, respectively; $[X_f]$ is the concentration of free AMPPNP, equal to $[X_f]=[X_T]/(1+2*k*[M_{2,f}]+2*k^2*[M_{2,f}]*[X_f])$; $[M_{2,f}]$ is the concentration of free MutL dimer, equal to $[M_{2,f}] = [M_T]/(1+2*k*[X_f]+k^2*[X_f]^2)$.

For DNA binding experiments (total DNA concentration, $[D_t]$ = 1.4 μM), the dependence of $\bar{s}_{app}$ on total [MutL dimer] ($[M_{2,T}]$) was analyzed using a 1:1 binding isotherm model to obtain an apparent association equilibrium constant, $K = 1/K_d$. Data were fitted implicitly to equation (6) using a Scientist program (Micromath, St. Louis, MO), where K is an apparent association constant; $[M_{2,f}]$ is the concentration of free

$$\bar{s}_{app} = \frac{A*K*[M_{2,f}]+B}{1+K*[M_{2,f}]} \quad (6)$$

MutL dimer, $[M_{2,f}] = [M_{2,T}]/(1+K*[D_f]$; $[D_f]$ is the concentration of free DNA, equal to $[D_f] = [D_T]/(1+K*[M_{2,f}])$; A is the sedimentation coefficient of the MutL-DNA complex, and B is the sedimentation coefficient of free DNA.

Results

Assembly state of MutL

A goal of these studies was to determine a set of solution conditions that enable us to study both MutL and UvrD separately and together in the presence and absence of a suitable DNA substrate. Towards this end we performed a series of sedimentation velocity experiments to evaluate the oligomeric state of MutL in a variety of buffers and protein concentrations. In the absence of DTT or 2-mercaptoethanol, we observed that a substantial fraction of MutL became covalently cross-linked via disulfide bond formation as detected by SDS-PAGE (data not shown). This cross-linking can be reversed by treatment with DTT or 2-mercaptoethanol (at mM concentrations). For this reason all further experiments were performed in the presence of 1 mM 2-mercaptoethanol. Previous experiments from our laboratory which characterized the self-association properties and helicase activity of UvrD were performed in a Tris buffer (28, 29, 59). Therefore, we first investigated the self association properties of MutL under these same solution conditions, but including 1 mM 2-mercaptoethanol (buffer TGN 10/20/20, Table 1). Under these conditions, MutL displays a very broad and non symmetrical c(s) distribution (Figure 1). Analysis of the c(s) distribution (49, 50) in buffer TGN 10/20/20, suggests that MutL exists as a heterogeneous mixture of species with sedimentation coefficients ranging from ~ 4.5 S (less than 8 % of all species) for the smallest species to larger species with 10 – 55 S (Figure 1A). Under these conditions, we estimate a weight average sedimentation coefficient of $\bar{s}_{20,w}$ = 29.1 S at 2 μM MutL (total monomer concentration). Upon increasing the [NaCl] in the TGN buffer from 20 mM to 100 mM, $\bar{s}_{20,w}$ decreased to 17.8 S at the same protein concentration, with approximately 28% of the MutL having $s_{20,w}$ = 4.5 S, indicating a reduction in the average size of the oligomeric species (Figure 1A).

We next examined a buffer used by the Modrich laboratory (39) to study the MutL assembly state by sucrose gradient centrifugation and that we use to store our MutL preparations. This buffer (Buffer M, Table 1) contains 50 mM potassium phosphate (pH 7.4 at 25°C), 50 mM KCl, 0.1 mM EDTA, 1 mM 2-mercaptoethanol. In Buffer M (25°C), the c(s) distribution displayed one major symmetrical peak with $s_{20,w}$ = 5.18 ± 0.03 S (Figure 1A), suggesting that MutL exists primarily as a single species (97% ± 2%). Therefore, the solution conditions have a profound influence on the self-association properties of MutL. Buffer M contains potassium instead of sodium and phosphate instead of Tris and does not contain any glycerol. To assess the effect of individual buffer constituents on the assembly state of MutL, we performed centrifugation experiments while systematically varying each component (Figure 1B and data not shown).

In the presence of 20% (v/v) glycerol and 20 mM NaCl in potassium phosphate buffer (buffer M20/20, Table 1), MutL displayed c(s) distribution profiles similar to its behavior in Buffer M (see Figure 1B and Figure 5B for experiments at 5°C and 25°C, respectively). In buffer M20/20 at 5°C, the c(s) distribution shows a major symmetrical peak at $s_{20,w}$ ~ 4.5 S (96% of total protein) and a minor peak at $s_{20,w}$ ~ 7.4 S (3.5 %), as well as minute quantities (0.06 %) of some larger species suggesting that the glycerol and NaCl in buffer TGN

10/20/20 do not facilitate MutL aggregation (see below and Figure 5). Replacing potassium phosphate with sodium phosphate at pH 7.4 (buffer N20/20, Table 1) also does not affect the self association properties of MutL ($\bar{s}_{20,w}$ = 4.60 ± 0.02 S, data not shown). Increasing the pH of buffer M from 7.4 to 8.3 also did not influence the sedimentation properties of MutL significantly ($\bar{s}_{20,w}$ = 4.79 ± 0.02 S, with ~ 6% of protein sedimented with higher $s_{20,w}$, data not shown). We also observed that lower temperatures reduced further aggregation of MutL, such that, even in Buffer TGN 10/20/20 at 5°C around 32% of the protein sedimented with $s_{20,w}$ = 4.8 S at a concentration of 3.2 μM monomer (buffer TGN 10/20/20, compare Figure 1B and Figure 1A). Substitution of potassium phosphate in buffer M with Tris (10 mM) (buffer M+Tris, Table 1) facilitated MutL self assembly beyond the ~ 4.5 S species (Figure 1B). For example, in buffer M+Tris at pH 8.3 (value of pH at 25°C) 94% of MutL sedimented with $s_{20,w}$ from 7.5 S – 45 S ($\bar{s}_{20,w}$ = 16.5 S), whereas at pH 7.4 (value of pH at 5°C) around 62 % of MutL sedimented at $s_{20,w}$ = 5.6 S with the rest of the protein sedimenting as a distribution of larger species (~ 9 S to 50 S), with $\bar{s}_{20,w}$ = 9.4 S (Figure 1B).

These experiments suggest that it is primarily the presence of PO_4^{-3} in Buffer M that shifts the distribution of MutL oligomeric species to favor the smaller species. To estimate the molecular weight of this smallest MutL species, we analyzed the sedimentation velocity experiments by non-linear least-squares (NLLS) methods using the program SEDFIT (see Material and Methods) (49). From the best-fit values of sedimentation and diffusion coefficients the molecular weight can be estimated using the Svedberg equation (Eq. 3, Material and Methods). The absorbance profiles were analyzed according to a two species model, to account for a small amount (up to 3%) of a higher order oligomeric species present in the MutL population, returning M_{app} = 112 ± 5 kDa for the major species, suggesting a dimeric form of MutL (predicted molar weight of MutL dimer is equal to 135.8 kDa). Additional experiments showed no dependence of $\bar{s}_{20,w}$ on [MutL] (Figure 2A), indicating that over the range studied (0.25 – 4 μM monomer), MutL exists as a single species, with $\bar{s}_{20,w}$ = 5.20 ± 0.08 S. Based on this value, we estimate a frictional coefficient ratio, f/f_o= 1.58 ± 0.02 using Eq. (4) (Materials and Methods), where f/f_o is the ratio of the frictional coefficient of the macromolecule to the frictional coefficient of a hydrated sphere of identical molecular weight. This suggests that the MutL dimer is highly asymmetric under these solution conditions.

MutL possesses a weak ATPase activity that is stimulated several fold by ssDNA (24). It has been suggested that the binding of AMPPNP, a non hydrolysable ATP analogue, would induce a partial folding and dimerization of the N-terminus of MutL (38). We therefore examined the effect of AMPPNP on the self association properties of MutL using sedimentation velocity. MutL was dialyzed into Buffer M, containing 1 mM $MgCl_2$, and then equilibrated with AMPPNP (35 μM) for 1 hour at 25°C before centrifugation. The addition of AMPPNP increased $\bar{s}_{20,w}$ from 5.20 ± 0.08 S to 5.71 ± 0.08 S, independent of [MutL] (Figure 2A). Using the program SEDFIT, a molecular weight of 112 ± 6 kDa was calculated for MutL, which is identical (within our uncertainty) to the value estimated in the absence of AMPPNP and $MgCl_2$. Experiments performed in buffer M + 1 mM $MgCl_2$ yielded an $\bar{s}_{20,w}$ that was similar to the value determined in the absence of AMPPNP and $MgCl_2$. Therefore, the increase in $s_{20,w}$ is solely due to AMPPNP binding to MutL (Figure 2B and data not shown). These results suggest that AMPPNP binding does not affect the oligomeric state of MutL, but rather its hydrodynamic shape such that the dimer becomes more compact, with f/f_o = 1.45 ± 0.02.

In order to estimate the apparent affinity of AMPPNP for the MutL dimer we performed a series of sedimentation velocity experiments at constant MutL protein (1.75 μM dimer loading concentration) as a function of [AMPPNP] (Buffer M + 1mM $MgCl_2$). Figure 2B

shows that $\overline{s}_{20,w}$ increases with [AMPPNP]. NLLS analysis of the data using a model that assumes two identical and independent AMPPNP binding sites per MutL dimer (Eq. (5) in Material and Methods) yields a binding constant of 3.9 (± 1.1) $\times 10^4$ M^{-1}.

To further test whether the predominant assembly state of MutL is a dimer in its apo and AMPPNP/Mg^{2+} bound form, we performed sedimentation equilibrium studies in Buffer M (Figure 3). Experiments were conducted at 5°C in order to suppress aggregation of MutL beyond the smallest oligomeric state during the extended time of these experiments. Data were obtained at 4 rotor speeds (12,000; 15,000 19,000 and 23,000 rpm) and several MutL loading concentrations. The data were first analyzed individually by non-linear, least-squares (NLLS) methods using a single ideal species model (n = 1 in Eq. 1, Material and Methods) to estimate the weight average buoyant molecular mass ($\overline{M}_b = \overline{M}(1-\overline{\upsilon}\,\rho)$). At each loading concentration, the resulting $\overline{M}_b$ was equal to that expected for a MutL dimer (Figure 3). Similar results were obtained for MutL dialyzed against buffer M + 1mM $MgCl_2$ and in the presence of 35 μM AMPPNP (data not shown). All of the data were then fitted globally by NLLS methods, using a single ideal species model (n = 1 in Eq. 1, Material and Methods) and assuming a partial specific volume, $\overline{\upsilon}_{5°C}$ = 0.7329 ml/g, for MutL (estimated from the amino acid composition of MutL (47) and Eq. (2)). Representative data sets obtained in buffer M (1.9, 0.95, 0.475 μM monomer) and buffer M + 35 μM AMPPNP + 1mM $MgCl_2$ (2.77, 1.38, 0.69 μM monomer) are shown in Figure 4A and Figure 4B, respectively. For apo MutL the calculated molar mass, M = 130.5 ± 3.0 kDa, is only ~4% lower than that expected for the MutL dimer (M_{MutL2} = 135.8 kDa). Similar results were obtained in buffer M + 1 mM $MgCl_2$ and 35 μM AMPPNP, with a calculated molar mass, M = 131.9 ± 4.2 kDa, (predicted $M_{MutL2\text{-}AMPPNP}$ = 136.8 kDa). These results are consistent with MutL being a stable dimer with extended shape, which becomes more compact upon binding a non-hydrolysable ATP analogue.

Unfortunately, in buffer M, UvrD forms large complexes that cannot be studied easily in the centrifuge. The distribution of UvrD assembly states is sensitive to [NaCl] and [glycerol] (28, 60). However, we have been able to determine a set of conditions in which the assembly states of both UvrD and MutL can be studied and that supports helicase activity (buffer M20/20, Table 1). Sedimentation equilibrium experiments with MutL were therefore repeated in buffer M20/20 at 25°C, at four rotor speeds (12,000 rpm, 15,000 rpm, 19,000 rpm and 23,000 rpm) and three [MutL] (2.64, 1.32, 0.66 μM monomer loading concentrations) (Figure 5A). These data were fitted globally to a single ideal species model (Material and Methods) returning M = 120.0 ± 5.7 kDa, which is ~9 % – 11 % lower than that expected for a MutL dimer (Figure 5A). Models taking into account hydrodynamic non-ideality or monomer-dimer self-association equilibrium did not improve the quality of the fit and parameters were not constrained (not shown). However, we noticed that $\overline{M}_b$ deviated to a larger extent for higher rotor speeds (longer centrifugation time) and higher [MutL]. This observation prompted us to repeat the NLLS fitting for concentration profiles obtained at the two lowest rotor speeds, which yielded M = 130.2 ± 6.9 kDa, which is the value expected for the MutL dimer. This result suggests that there is some MutL heterogeneity in buffer M20/20. To further test this idea we conducted sedimentation velocity studies in buffer M20/20 (50, 61). The c(s) distribution calculated for MutL in buffer M20/20 at 25°C displayed one main peak with a symmetrical shape at $s_{20,w}$ = 4.75 ± 0.02 S (Figure 5B), although an additional minor species (~ 4%) with a broad peak at $s_{20,w} \approx 7.6 \pm 0.2$ S was also present. The $\overline{s}_{20,w}$, calculated by integration of c(s) over both peaks, increases slightly with increasing [MutL] with an average value of 4.88 ± 0.04 S (Figure 5C), yielding f/f_o = 1.69 ± 0.01. We conclude that in buffer M20/20 at 25°C MutL is an elongated dimer, accompanied by a minor population (4%) of larger aggregates that are not in equilibrium with the dimeric form under the conditions and over the time intervals used in our experiments.

Assembly state of MutL bound to DNA

Recent genetic and biochemical data strongly suggest that DNA binding by MutL is required for MMR *in vivo* (6, 62). Furthermore, MutL has been shown to stimulate the helicase activity of UvrD (22, 26, 62). DNA binding of MutL has been investigated previously using EMSA, nitrocellulose filter binding, surface plasmon resonance and by following the stimulation of the ATPase activity of MutL in the presence of a DNA cofactor (7, 9, 25, 26, 38, 62–64). Here we investigated the DNA binding properties of MutL on the DNA substrate that we have used previously to study the helicase activity of UvrD (20, 29, 30, 34) using sedimentation velocity and equilibrium techniques. The DNA consisted of an 18 bp duplex possessing a 3'-dT_{20} tail with a Cy3 chromophore attached covalently to the blunt DNA end via the 5' end (3'(dT_{20})-ds18-Cy3). Using the Cy3 label as a reporter, one can monitor the sedimentation profile of the DNA via the absorbance of the Cy3 chromophore (at 550 nm) without interference from MutL. Experiments were performed at different ratios of MutL dimer to DNA in buffer M20/20 at 25°C (Figure 6).

The resulting uncorrected c(s) distributions (50, 65) show two well resolved, symmetrical peaks at 1.15 ± 0.02 S and 2.35 ± 0.03 S (Figure 6A). The position of the second peak did not change with increasing [MutL] suggesting that they represent distinct MutL-DNA species (66, 67). The first peak at 1.15 ± 0.02 S represents free DNA (black curve, Figure 6A). The second peak near 2.35 S represents MutL-DNA complexes. An apparent binding isotherm was constructed by plotting the weight average sedimentation coefficient as a function of the molar ratio of the MutL dimer to DNA (Figure 6B) (52, 68). This binding isotherm was analyzed assuming that a single MutL dimer binds to each DNA substrate (see below), yielding an apparent binding constant of 34 (±4.3) × 10^4 M^{-1} (Eq. 6 in Material and Methods). The smooth curve in Figure 6B is a simulation using the best fit parameters derived from the NLLS fit of the data to a 1:1 binding isotherm. These data suggest that MutL has low affinity towards DNA and does not bind stoichiometrically under our experimental conditions (i.e., not all added MutL forms a complex with the DNA).

To determine the molecular weight of the MutL-DNA complex corresponding to the 2.35 S species, we performed a sedimentation equilibrium experiment. Figure 6C shows a representative set of concentration profiles collected in buffer M20/20 at 25°C at five different rotor speeds for a 2.34-fold molar excess of MutL dimer over 3'(dT_{20})-ds18-Cy3 DNA. These absorbance profiles were analyzed using a two species model, one corresponding to the free Cy3-labelled DNA, and the other to a MutL-DNA complex. The buoyant molecular mass (M_b) of the Cy3-DNA was fixed at 6.66 (± 0.22) kg mol^{-1} based on independent sedimentation equilibrium experiments performed on the free DNA (Material and Methods). From NLLS analysis of the data in Figure 6C we obtain a best fit value of M_b = 39.61 ± 0.46 kg mol^{-1} for the MutL-DNA complex. This value is only slightly higher than the buoyant molecular mass expected for a single MutL dimer bound to the Cy3-DNA molecule (M_2D), $M_{b,M2D}$ = 35.56 kg mol^{-1} (Material and Methods). When the experiment was repeated at a 1.25 fold molar excess of the MutL dimer over DNA, we obtained M_b = 39.16 ± 0.76 kg mol^{-1} in agreement with the higher molar ratio data. Including an additional species in the NLLS analysis did not improve the quality of the fit and resulted in unconstrained fitting parameters (data not shown). Thus, over the concentration range studied, these results indicate that a single MutL dimer binds to a 3'(dT_{20})-ds18 DNA.

Based on the stoichiometry of the MutL-DNA complex (M_2D) we calculated a weight average partial specific volume, $\bar{\upsilon}_{MutL2\text{-}DNA}$ = 0.7237 ml/g at 25°C (Eq. 2, Material and Methods) for a single MutL dimer bound to the DNA. This can be used to correct the value of the apparent sedimentation coefficient of the M_2D complex to standard conditions ($s_{20,w}$, see Material and Methods) and obtain an estimate of the frictional coefficient ratio for the M_2D complex (Eq. 4, Material and Methods). For the MutL dimer bound to the 3'(dT_{20})-

ds18-Cy3 DNA, we obtain $s_{20,w}$ = 5.00 ± 0.06 S, and f/f_o = 1.90 ± 0.02, which suggests that the M_2D complex is quite asymmetric.

MutL-DNA complexes in the presence of AMPPNP

It was reported previously that MutL displays enhanced DNA binding activity in the presence of AMPPNP (6, 26, 38, 62). An apparent binding constant of 4×10^7 M^{-1} was measured for MutL binding to DNA (93 nt primer annealed to M13 ssDNA) in 25 mM Tris (pH 7.5 at 22°C), 20 mM NaCl, 3 mM $MgCl_2$, 5 mM 2-mercapthoethanol, 50 μg/ml BSA, whereas a ten-fold higher binding constant of 36×10^7 M^{-1} was measured in the presence of 3 mM AMPPNP (26, 62). Moreover, it was suggested that an ATP-bound form of MutL continuously loads UvrD onto a DNA substrate (6, 21). In light of these results, and considering the AMPPNP induced conformational change of MutL (see above) it was of interest to study the hydrodynamic properties and stoichiometry of the ternary MutL-AMPPNP-DNA complex. Sedimentation velocity experiments were performed at different ratios of MutL to 3'(dT_{20})-ds18-Cy3 DNA in the presence or absence of 0.4 mM AMPPNP in buffer M20/20 at 25°C (Figure 7).

A representative data set obtained at a ratio of 1 MutL dimer per DNA is shown in Figure 7A. Plotting the $\overline{s}_{app}$ as a function of [MutL] in the presence or absence of 0.4 mM AMPPNP shows that AMPPNP enhances MutL binding affinity towards 3'(dT_{20})-ds18-Cy3 DNA (Figure 7B), and yields an apparent binding constant of 38 (± 2.5) × 10^5 M^{-1} (Eq. 6 in Material and Methods). In the absence of AMPPNP, MutL binding to DNA is 20-fold weaker with an apparent binding constant of 1.96 (± 0.2) × 10^5 M^{-1} (Figure 7B). These results show that the increase M_2D complex formation is due to AMPPNP binding to MutL. MutL, in the presence of both Mg^{2+} and AMPPNP forms a stable, well defined protein-DNA species, since the position of the peak reflecting the MutL-DNA complex does not change with increasing protein concentrations (data not show). Analogous behavior was also observed in buffer M20/20 (Figure 6A), which suggests that the MutL-DNA equilibrium dynamics are slow in comparison to the time scale of sedimentation velocity (52, 66, 67). In the presence of 1 mM $MgCl_2$ in buffer M20/20, for all [MutL] studied the c(s) distributions show two well resolved and symmetrical peaks centered at 1.14 ± 0.02 S and 2.36 ± 0.02 S (Figure 7A), consistent with what was observed in buffer M20/20 (Figure 6A), suggesting that a single MutL dimer binds per 3'(dT_{20})-ds18-Cy3 DNA. The values of the sedimentation coefficients corrected to standard conditions are $s_{20,w}$ = 2.23 S ± 0.02 for DNA and $s_{20,w}$ = 5.02 S ± 0.05 for the M_2D complex, similar to the values in buffer M20/20, suggesting a similar hydrodynamic shape for both macromolecular species.

In the presence of 1 mM $MgCl_2$ + 0.4 mM AMPPNP (buffer M20/20), the two well resolved and symmetrical c(s) peaks are centered at 1.16 ± 0.01 S and 2.82 ± 0.02 S (Figure 7A and data not shown) which, upon correction to standard conditions, yields $s_{20,w}$ = 2.25 S ± 0.03 for DNA and $s_{20,w}$ = 5.99 S ± 0.05 for the MutL-DNA-AMPPNP ternary complex (M_2D-AMPPNP). The $s_{20,w}$ for M_2D-AMPPNP complex is higher than that of the M_2D complex in the presence and absence of Mg^{2+}. The calculated frictional coefficient ratio (Eq. 4, Material and Methods) for the ternary complex is f/f_o = 1.61 ± 0.01, which is lower than the value in the absence of nucleotide (1.90 ± 0.02, see above), suggesting that the M_2D complex becomes more compact upon AMPPNP binding (24, 38). Sedimentation velocity experiments performed at a 1:1 molar ratio of MutL dimer to Cy3-DNA (buffer M20/20 + 1mM $MgCl_2$), as a function of [AMPPNP] (Supplemental Figure 1), shows that the concentration of the nucleotide cofactor used in our studies (400 μM) is saturating. Data in Supplemental Figure 1 were analyzed using a model that assumes two identical and independent AMPPNP binding sites per MutL dimer (Eq. (5) in Material and Methods), returning an apparent binding constant of 7.0 (± 2.8) ×10^4 M^{-1}.

Discussion

Knowledge of the assembly state of any enzyme is needed to fully understand the molecular mechanism of its function and to facilitate interpretation of the thermodynamics of its interactions with its substrates and cofactors. In previous studies a range of assembly states of full length MutL has been observed using a variety of approaches including glycerol gradient centrifugation, gel filtration chromatography and dynamic light scattering techniques (7, 39). In 50 mM potassium phosphate, pH 7.4, 50 mM KCl, 0.1 mM EDTA, 1 mM DTT at 3°C, MutL was found to have $s_{20,w}$ = 5.5 S and a Stokes radius of 61 Å, suggesting a dimer with an asymmetric shape (f/f_o = 1.8) (39). Dynamic light-scattering experiments performed at 24°C in 20 mM Tris (pH 8.0), 200 mM KCl, 5 mM $MgCl_2$, 1 mM DTT, 0.1 mM EDTA suggested that MutL has a Stokes radius of 86 Å which decreases to 56 Å upon binding of AMPPNP (7). The dimensions of the MutL dimer calculated from these two studies differ substantially. This difference could result from differences in protein concentration or solution conditions (i.e., buffer composition and/or temperature) used in the two studies. Changes in any of these parameters can potentially influence the MutL assembly state as we have shown here.

MutL can self-associate to form high order oligomeric species

Our sedimentation velocity analysis of MutL shows that solutions without phosphate promotes MutL to self-associate into larger heterogeneous oligomeric species. The extent of the MutL heterogeneity, and the average size of the species formed, were both reduced at lower temperatures, lower protein concentrations and higher [NaCl]. Ban and Yang (24) noted previously that the full length MutL "tends to aggregate", although this self-association process was not studied further.

The structure of the MutL C-terminal 20 kDa domain shows a dimer whereas the N-terminal domain is monomeric in the absence of nucleotide, but forms a dimer when bound to AMPPNP (24, 38). A model based on the crystal structures proposes that MutL forms a stable dimer through its C-terminal domains connected to their respective N-terminal domains by unstructured linkers which undergo ATP-dependent conformational changes leading to communication with MutS and MutH during mismatch repair (7). The propensity of MutL to self-associate beyond a dimer may be due to the partially unfolded and "monomeric" state of the N-terminal domain (38). The observation that the MutL-AMPPNP complex forms more stable dimers in solution (24) supports this idea. Interestingly, in buffer M (Table 1) for loading concentrations of 0.2 – 5 μM monomer we detect only dimers of MutL (Figure 2 and 3). Furthermore, MutL remains dimeric over a similar concentration range in buffer M containing 10 mM to 1M KCl or in the presence of 20% (v/v) glycerol, suggesting that a dimer is a stable oligomeric state of MutL. Buffer M was used previously by Modrich and coworkers for purification, storage and preliminary characterization of MutL (39) and our results are consistent with their studies of the MutL assembly state under these conditions.

The dimeric state of MutL observed in buffer M is in sharp contrast to the highly heterogeneous distribution of multimeric species observed in Tris buffers. Our sedimentation velocity experiments suggest that the presence of phosphate at pH 7.4 stabilizes the MutL dimer relative to these higher order aggregates. Since MutL is an ATPase, it is possible that PO_4^{-3}, which is one of the products of ATP hydrolysis, binds to the ATP binding pocket and stabilizes the disordered surfaces in apo MutL, such that the protein is no longer prone to further self-association beyond a dimer. Even if this is the case, the N-termini of MutL do not fully fold and/or dimerize in buffer containing potassium phosphate as it is observed only upon AMPPNP binding.

Monovalent cations such as sodium and potassium may also contribute to MutL stability by stabilizing the conformation of the ATP pocket lid. In addition to magnesium which is essential for catalysis, a potassium ion is observed to be bound adjacent to the triphosphate moiety of ADPNP in the crystal structure of N-terminal 40 kDa fragment of MutL (69). The potassium ion is coordinated by four carbonyl oxygen atoms that originate from amino acids located at the N-terminal hinge of the ATP lid, and a water molecule, such that the monovalent cation may stabilize the ATP pocket lid (69).

Hydrodynamic properties of MutL dimers

We performed both sedimentation velocity and equilibrium experiments over a wide range of [MutL] (0.25 – 5 μM monomer), under identical solution conditions in the absence and presence of the non-hydrolysable ATP analogue - AMPPNP. Analysis of the sedimentation equilibrium data unequivocally shows that apo and AMPPNP-bound MutL are dimeric in buffer M (5°C and 25°C). From the sedimentation coefficient of MutL ($\bar{s}_{20,w}$ = 5.20 ± 0.08 S for nucleotide free and $\bar{s}_{20,w}$ = 5.71 ± 0.08 S for AMPPNP-bound MutL dimer) we can calculate the f/f_o ratio (Material and Methods, Eq. 4) (28, 53, 54), which reflects the overall shape of the protein(52, 70). For apo and AMPPNP-bound MutL these differ substantially with f/f_o = 1.58 ± 0.02 and 1.45 ± 0.02, respectively. These values indicate that both dimers are highly extended and/or possess disordered/unfolded regions (53, 70, 71). However, upon binding of AMPPNP the overall shape of the MutL dimer changes. In light of the available crystal structures of the N-terminal fragment of MutL we suggest that this reflects the folding and dimerization of the partially disordered “monomeric” N-termini of the MutL dimer, resulting in a more compact structure. Similar hydrodynamic parameters for the MutL dimer were obtained in buffer M20/20 ($\bar{s}_{20,w}$ = 4.88 ± 0.04 S and f/f_o = 1.69 ± 0.01). Our results are in good agreement with values reported by Modrich and coworkers (39). The differences between those results and other studies (7) is likely due to the lack of phosphate in the latter experiments, conditions which we have shown here to facilitate further aggregation of MutL beyond a dimer.

Stoichiometry and hydrodynamic properties of a MutL-DNA complex

We also examined the stoichiometry of MutL bound to a 3’(dT_{20})-ds18 DNA in buffer M20/20 ± 1mM $MgCl_2$ as well as in the presence of 1mM $MgCl_2$ and 0.4 mM AMPPNP. In a 2.5 molar excess of MutL dimer over DNA we detect a single species composed of one MutL dimer bound to one DNA molecule. In the presence of 1 mM $MgCl_2$, $s_{20,w}$ = 5.02 S ± 0.05 for the M_2D complex, yielding f/f_o = 1.90 ± 0.02 (similar values were obtained without $MgCl_2$). In the presence of 1 mM $MgCl_2$ and 0.4 mM AMPPNP, a distinct ternary complex is formed with $s_{20,w}$ = 5.99 S ± 0.05 S, yielding f/f_o = 1.61 ± 0.01. Our results suggest that upon binding AMPPNP, the highly asymmetrical M_2D complex becomes more compact, likely due to the folding and dimerization of the N-termini of MutL and concomitant closure of the central channel possibly encircling the DNA. This conformational change has not previously been observed, although it was postulated based on molecular modeling of the full length MutL (7, 38).

Although in buffer M20/20 MutL binds weakly to 3’(dT_{20})-ds18 DNA (apparent binding constant: 34 (±4.3) × 10^4 M^{-1}), and the presence of 1 mM $MgCl_2$ further weakens the interaction (~ 2-fold), in the presence of 0.4 mM AMPPNP + 1 mM $MgCl_2$, the binding increases by an order of magnitude (apparent binding constant: 38 (± 2.5) × 10^5 M^{-1}). In the crystal structure of the dimeric N-terminal MutL fragment bound to AMPPNP a deep, saddle-shaped groove with high positive electrostatic surface potential is formed between two subunits which can accommodate ss DNA (38). It was proposed that this saddle constitutes a DNA binding site and this proposal is supported by mutational analysis (6, 25, 38, 62). Previous filter binding studies performed in 25 mM Tris, pH 7.5, 100 mM NaCl, 3

mM $MgCl_2$, 5 mM 2-mercapthoethanol and 3 mM AMPPNP at 37°C estimated a binding constant of 24×10^4 M^{-1} for MutL binding to a 50 bp duplex with a 20 nucleotide 3' overhang (62). In our studies, we have measured an apparent binding constant of 38 (± 2.5) $\times 10^5$ M^{-1} for MutL binding to an 18 bp duplex with a 3'$(dT)_{20}$ tail (Cy3-labeled). These differences likely reflect differences in solution conditions, DNA and the methods employed to measure affinity.

Recently, a computational analysis of all protein interfaces observed in the crystal structure of the C-terminal domain of MutL was reported (72). Based on this it was suggested that the biologically relevant dimer interface is different from the one proposed in the original report (7), leading to a revised model of full-length MutL (72) that seems compatible with the results of crosslinking experiments. Deletion of the C-terminal 10 amino acid residues of MutL, which form part of the interface in the revised dimer inhibits dimer formation based on gel filtration experiments (72). In another study, a dimeric structure for a similar deletion was observed both in gel filtration and analytical ultracentrifugation experiments (21), which would suggest that the originally proposed interface is correct. The origin of this discrepancy is not clear, although it may be that the high salt concentration (500 mM NaCl and separation of MutL oligomeric species in size exclusion chromatography) used in the former study (72) may facilitate dimer disruption. Our data show that MutL has an elongated hydrodynamic shape that in principle agrees with both models. Mutagenic analysis of these predicted dimerization interfaces is required to further probe the oligomeric nature of MutL.

Supplementary Material

Refer to Web version on PubMed Central for supplementary material.

Acknowledgments

We thank Paul Modrich (Duke University) for providing the MutL overexpression plasmid and Thang Ho for synthesis and purification of oligodeoxynucleotides..

This research was supported by a NIH grant to TML (GM45948)

Abbreviations

MMR	methyl-directed mismatch repair
SF1	superfamily 1
NLLS	Non-linear least squares

References

1. Iyer RR, Pluciennik A, Burdett V, Modrich PL. DNA mismatch repair: functions and mechanisms. Chem Rev. 2006; 106:302–323. [PubMed: 16464007]
2. Hsieh P. Molecular mechanisms of DNA mismatch repair. Mutat Res. 2001; 486:71–87. [PubMed: 11425513]
3. Kunkel TA, Erie DA. DNA mismatch repair. Annu Rev Biochem. 2005; 74:681–710. [PubMed: 15952900]
4. Yang W. Structure and function of mismatch repair proteins. Mutat Res. 2000; 460:245–256. [PubMed: 10946232]
5. Su SS, Modrich P. Escherichia coli mutS-encoded protein binds to mismatched DNA base pairs. Proc Natl Acad Sci U S A. 1986; 83:5057–5061. [PubMed: 3014530]

6. Robertson AB, Pattishall SR, Gibbons EA, Matson SW. MutL-catalyzed ATP hydrolysis is required at a post-UvrD loading step in methyl-directed mismatch repair. J Biol Chem. 2006; 281:19949–19959. [PubMed: 16690604]
7. Guarne A, Ramon-Maiques S, Wolff EM, Ghirlando R, Hu X, Miller JH, Yang W. Structure of the MutL C-terminal domain: a model of intact MutL and its roles in mismatch repair. Embo J. 2004; 23:4134–4145. [PubMed: 15470502]
8. Grilley M, Griffith J, Modrich P. Bidirectional excision in methyl-directed mismatch repair. J Biol Chem. 1993; 268:11830–11837. [PubMed: 8505311]
9. Acharya S, Foster PL, Brooks P, Fishel R. The coordinated functions of the E. coli MutS and MutL proteins in mismatch repair. Mol Cell. 2003; 12:233–246. [PubMed: 12887908]
10. Allen DJ, Makhov A, Grilley M, Taylor J, Thresher R, Modrich P, Griffith JD. MutS mediates heteroduplex loop formation by a translocation mechanism. Embo J. 1997; 16:4467–4476. [PubMed: 9250691]
11. Junop MS, Obmolova G, Rausch K, Hsieh P, Yang W. Composite active site of an ABC ATPase: MutS uses ATP to verify mismatch recognition and authorize DNA repair. Mol Cell. 2001; 7:1–12. [PubMed: 11172706]
12. Yang W, Junop MS, Ban C, Obmolova G, Hsieh P. DNA mismatch repair: from structure to mechanism. Cold Spring Harb Symp Quant Biol. 2000; 65:225–232. [PubMed: 12760036]
13. Matson SW. Escherichia coli helicase II (urvD gene product) translocates unidirectionally in a 3' to 5' direction. J Biol Chem. 1986; 261:10169–10175. [PubMed: 2942537]
14. Georgi-Geisberger P, Hoffmann-Berling H. Direction of the DNA-unwinding reaction catalysed by Escherichia coli DNA helicase II. Eur J Biochem. 1990; 192:689–693. [PubMed: 2170128]
15. Runyon GT, Bear DG, Lohman TM. Escherichia coli helicase II (UvrD) protein initiates DNA unwinding at nicks and blunt ends. Proc Natl Acad Sci U S A. 1990; 87:6383–6387. [PubMed: 2166955]
16. Dao V, Modrich P. Mismatch-, MutS-, MutL-, and helicase II-dependent unwinding from the single-strand break of an incised heteroduplex. J Biol Chem. 1998; 273:9202–9207. [PubMed: 9535911]
17. Burdett V, Baitinger C, Viswanathan M, Lovett ST, Modrich P. In vivo requirement for RecJ, ExoVII, ExoI, and ExoX in methyl-directed mismatch repair. Proc Natl Acad Sci U S A. 2001; 98:6765–6770. [PubMed: 11381137]
18. Viswanathan M, Burdett V, Baitinger C, Modrich P, Lovett ST. Redundant exonuclease involvement in Escherichia coli methyl-directed mismatch repair. J Biol Chem. 2001; 276:31053–31058. [PubMed: 11418610]
19. Lahue RS, Au KG, Modrich P. DNA mismatch correction in a defined system. Science. 1989; 245:160–164. [PubMed: 2665076]
20. Ali JA, Lohman TM. Kinetic measurement of the step size of DNA unwinding by Escherichia coli UvrD helicase. Science. 1997; 275:377–380. [PubMed: 8994032]
21. Matson SW, Robertson AB. The UvrD helicase and its modulation by the mismatch repair protein MutL. Nucleic Acids Res. 2006; 34:4089–4097. [PubMed: 16935885]
22. Yamaguchi M, Dao V, Modrich P. MutS and MutL activate DNA helicase II in a mismatch-dependent manner. J Biol Chem. 1998; 273:9197–9201. [PubMed: 9535910]
23. Hall MC, Jordan JR, Matson SW. Evidence for a physical interaction between the Escherichia coli methyl-directed mismatch repair proteins MutL and UvrD. Embo J. 1998; 17:1535–1541. [PubMed: 9482750]
24. Ban C, Yang W. Crystal structure and ATPase activity of MutL: implications for DNA repair and mutagenesis. Cell. 1998; 95:541–552. [PubMed: 9827806]
25. Junop MS, Yang W, Funchain P, Clendenin W, Miller JH. In vitro and in vivo studies of MutS, MutL and MutH mutants: correlation of mismatch repair and DNA recombination. DNA Repair (Amst). 2003; 2:387–405. [PubMed: 12606120]
26. Mechanic LE, Frankel BA, Matson SW. Escherichia coli MutL loads DNA helicase II onto DNA. J Biol Chem. 2000; 275:38337–38346. [PubMed: 10984488]
27. Runyon GT, Lohman TM. Kinetics of Escherichia coli helicase II-catalyzed unwinding of fully duplex and nicked circular DNA. Biochemistry. 1993; 32:4128–4138. [PubMed: 8471620]

28. Maluf NK, Lohman TM. Self-association equilibria of Escherichia coli UvrD helicase studied by analytical ultracentrifugation. J Mol Biol. 2003; 325:889–912. [PubMed: 12527298]
29. Maluf NK, Fischer CJ, Lohman TM. A Dimer of Escherichia coli UvrD is the active form of the helicase in vitro. J Mol Biol. 2003; 325:913–935. [PubMed: 12527299]
30. Ali JA, Maluf NK, Lohman TM. An oligomeric form of E. coli UvrD is required for optimal helicase activity. J Mol Biol. 1999; 293:815–834. [PubMed: 10543970]
31. Lohman TM, Tomko EJ, Wu CG. Non-hexameric DNA helicases and translocases: mechanisms and regulation. Nat Rev Mol Cell Biol. 2008; 9:391–401. [PubMed: 18414490]
32. Heller RC, Marians KJ. Non-replicative helicases at the replication fork. DNA Repair (Amst). 2007; 6:945–952. [PubMed: 17382604]
33. Sun B, Wei KJ, Zhang B, Zhang XH, Dou SX, Li M, Xi XG. Impediment of E. coli UvrD by DNA-destabilizing force reveals a strained-inchworm mechanism of DNA unwinding. Embo J. 2008; 27:3279–3287. [PubMed: 19008855]
34. Fischer CJ, Maluf NK, Lohman TM. Mechanism of ATP-dependent translocation of E.coli UvrD monomers along single-stranded DNA. J Mol Biol. 2004; 344:1287–1309. [PubMed: 15561144]
35. Tomko EJ, Fischer CJ, Niedziela-Majka A, Lohman TM. A nonuniform stepping mechanism for E. coli UvrD monomer translocation along single-stranded DNA. Mol Cell. 2007; 26:335–347. [PubMed: 17499041]
36. Tomko EJ, Jia H, Park J, Maluf NK, Ha T, Lohman TM. 5'-Single-stranded/duplex DNA junctions are loading sites for E. coli UvrD translocase. Embo J. 2010; 29:3826–3839. [PubMed: 20877334]
37. Brendza KM, Cheng W, Fischer CJ, Chesnik MA, Niedziela-Majka A, Lohman TM. Autoinhibition of Escherichia coli Rep monomer helicase activity by its 2B subdomain. Proc Natl Acad Sci U S A. 2005; 102:10076–10081. [PubMed: 16009938]
38. Ban C, Junop M, Yang W. Transformation of MutL by ATP binding and hydrolysis: a switch in DNA mismatch repair. Cell. 1999; 97:85–97. [PubMed: 10199405]
39. Grilley M, Welsh KM, Su SS, Modrich P. Isolation and characterization of the Escherichia coli mutL gene product. J Biol Chem. 1989; 264:1000–1004. [PubMed: 2536011]
40. Fritsch, EF.; Sambrook, J.; Maniatis, T. Molecular Cloning: A laboratory Manual. Vol. Vol. 1. Pr New York: Cold Spring Harbor Laboratory; 1989.
41. Lohman TM, Chao K, Green JM, Sage S, Runyon GT. Large-scale purification and characterization of the Escherichia coli rep gene product. J Biol Chem. 1989; 264:10139–10147. [PubMed: 2524489]
42. Wong I, Chao KL, Bujalowski W, Lohman TM. DNA-induced dimerization of the Escherichia coli rep helicase. Allosteric effects of single-stranded and duplex DNA. J Biol Chem. 1992; 267:7596–7610. [PubMed: 1313807]
43. Kozlov AG, Lohman TM. Stopped-flow studies of the kinetics of single-stranded DNA binding and wrapping around the Escherichia coli SSB tetramer. Biochemistry. 2002; 41:6032–6044. [PubMed: 11993998]
44. Holbrook JA, Capp MW, Saecker RM, Record MT Jr. Enthalpy and heat capacity changes for formation of an oligomeric DNA duplex: interpretation in terms of coupled processes of formation and association of single-stranded helices. Biochemistry. 1999; 38:8409–8422. [PubMed: 10387087]
45. Laue, TM.; Shah, BD.; Ridgeway, TM.; Pelletier, SL. Computer-aided interpretation of analytical sedimentation data for proteins. Vol. Vol. 1. Cambridge, UK: Royal Society of Chemistry; 1992.
46. Johnson ML, Correia JJ, Yphantis DA, Halvorson HR. Analysis of data from the analytical ultracentrifuge by nonlinear least-squares techniques. Biophys J. 1981; 36:575–588. [PubMed: 7326325]
47. Cohn, EJ.; E, JT. Proteins, Amino Acids and Peptides as Ions and Dipolar Ions. Vol. Vol. 1. New York: Rheinhold; 1943. a.
48. Durchschlag, H. Specific volumes of biological macromolecules and some other molecules of biological interest. Vol. Vol. 1. New York: Springer-Verlag; 1986.
49. Schuck P. Sedimentation analysis of noninteracting and self-associating solutes using numerical solutions to the Lamm equation. Biophys J. 1998; 75:1503–1512. [PubMed: 9726952]

50. Dam J, Schuck P. Calculating sedimentation coefficient distributions by direct modeling of sedimentation velocity concentration profiles. Methods Enzymol. 2004; 384:185–212. [PubMed: 15081688]
51. Svedberg, T. The Ultracentrifuge. New York: Johnson Reprint Corporation; 1940.
52. Schuck, P. Difusion-Deconvoluted Sedimentation Coefficient Distributions for the Analysis of Interactin and Non-Interacting Protein Mixtures. Cambridge: The Royal Society of Chemistry; 2005.
53. Cantor, CR.; Schimmel, PR. Biophysical Chemistry. Part II: Techniques for the Study of Biological Structure and Function. twelfth ed.,. Vol. Vol. II. New York: W.H. Freeman and Company; 2002.
54. Bujalowski W, Klonowska MM, Jezewska MJ. Oligomeric structure of Escherichia coli primary replicative helicase DnaB protein. J Biol Chem. 1994; 269:31350–31358. [PubMed: 7989299]
55. Kuntz ID. Hydration of macromolecules. IV. Polypeptide conformation in frozen solutions. J Am Chem Soc. 1971; 93:516–518. [PubMed: 5541519]
56. Lin TH, Quinn T, Walsh M, Grandgenett D, Lee JC. Avian myeloblastosis virus reverse transcriptase. Effect of glycerol on its hydrodynamic properties. J Biol Chem. 1991; 266:1635–1640. [PubMed: 1703151]
57. Bastos M, Castro V, Mrevlishvili G, Teixeira J. Hydration of ds-DNA and ss-DNA by neutron quasielastic scattering. Biophys J. 2004; 86:3822–3827. [PubMed: 15189878]
58. Kuntz ID Jr, Kauzmann W. Hydration of proteins and polypeptides. Adv Protein Chem. 1974; 28:239–345. [PubMed: 4598824]
59. Maluf NK, Ali JA, Lohman TM. Kinetic mechanism for formation of the active, dimeric UvrD helicase-DNA complex. J Biol Chem. 2003; 278:31930–31940. [PubMed: 12788954]
60. Runyon GT, Wong I, Lohman TM. Overexpression, purification, DNA binding, and dimerization of the Escherichia coli uvrD gene product (helicase II). Biochemistry. 1993; 32:602–612. [PubMed: 8380701]
61. Laue T. Biophysical studies by ultracentrifugation. Curr Opin Struct Biol. 2001; 11:579–583. [PubMed: 11785759]
62. Robertson A, Pattishall SR, Matson SW. The DNA binding activity of MutL is required for methyl-directed mismatch repair in Escherichia coli. J Biol Chem. 2006; 281:8399–8408. [PubMed: 16446358]
63. Bende SM, Grafstrom RH. The DNA binding properties of the MutL protein isolated from Escherichia coli. Nucleic Acids Res. 1991; 19:1549–1555. [PubMed: 2027763]
64. Selmane T, Schofield MJ, Nayak S, Du C, Hsieh P. Formation of a DNA mismatch repair complex mediated by ATP. J Mol Biol. 2003; 334:949–965. [PubMed: 14643659]
65. Schuck P. Size-distribution analysis of macromolecules by sedimentation velocity ultracentrifugation and lamm equation modeling. Biophys J. 2000; 78:1606–1619. [PubMed: 10692345]
66. Dam J, Schuck P. Sedimentation velocity analysis of heterogeneous protein-protein interactions: sedimentation coefficient distributions c(s) and asymptotic boundary profiles from Gilbert-Jenkins theory. Biophys J. 2005; 89:651–666. [PubMed: 15863474]
67. Dam J, Velikovsky CA, Mariuzza RA, Urbanke C, Schuck P. Sedimentation velocity analysis of heterogeneous protein-protein interactions: Lamm equation modeling and sedimentation coefficient distributions c(s). Biophys J. 2005; 89:619–634. [PubMed: 15863475]
68. Correia JJ. Analysis of weight average sedimentation velocity data. Methods Enzymol. 2000; 321:81–100. [PubMed: 10909052]
69. Hu X, Machius M, Yang W. Monovalent cation dependence and preference of GHKL ATPases and kinases. FEBS Lett. 2003; 544:268–273. [PubMed: 12782329]
70. Tanford, C. Physical Chemistry of Macromolecules. New York: Wiley; 1961.
71. Teller DC, Swanson E, de Haen C. The translational friction coefficient of proteins. Methods Enzymol. 1979; 61:103–124. [PubMed: 481223]
72. Kosinski J, Steindorf I, Bujnicki JM, Giron-Monzon L, Friedhoff P. Analysis of the quaternary structure of the MutL C-terminal domain. J Mol Biol. 2005; 351:895–909. [PubMed: 16024043]

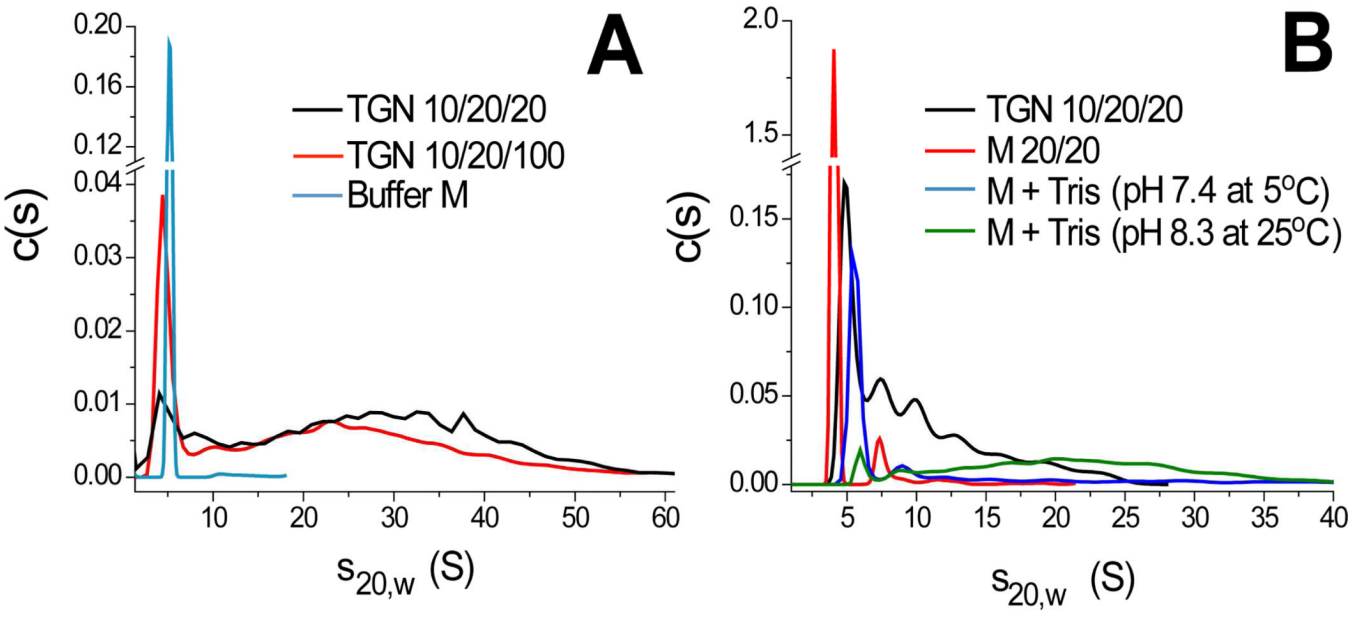

Figure 1.

Continuous sedimentation coefficient distribution c(s) analysis of MutL. MutL was dialyzed extensively into different buffers: TGN 10/20/20, TGN 10/20/100, buffer M, buffer M20/20, buffer M+Tris (Table 1). Dialyzed protein was sedimented at 30,000 rpm at loading concentration of 2 μM monomer at 25°C (**A**) or 3.2 μM monomer at 5°C (**B**). The absorbance scans were collected at 280 nm and analyzed using Sedfit, which approximate the mixture of macromolecular species as a system of non-interacting species with weight average frictional coefficient ratio $(f/f_o)_w$.

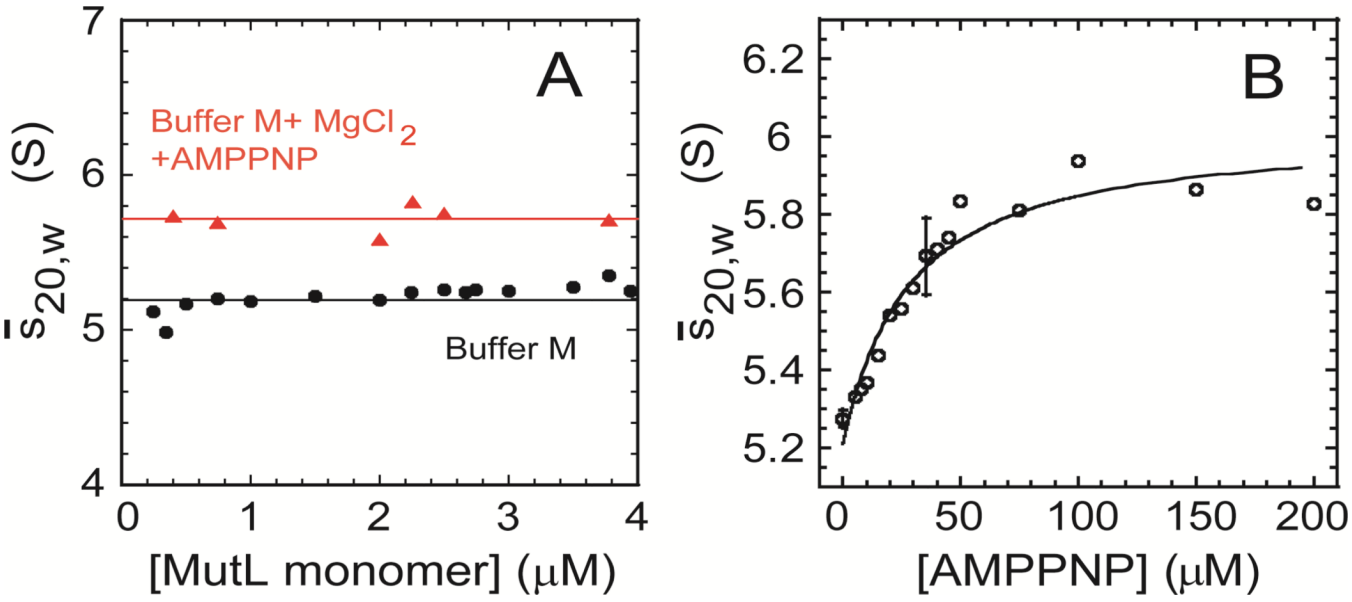

Figure 2.

Weight average sedimentation coefficient, $\bar{s}_{20,W}$, of MutL as a function of protein concentration (**A**) or [AMPPNP] included in the buffer (**B**). Sedimentation velocity experiments were performed at 25°C at different [MutL] (0.25 – 3.94 μM monomer loading concentration) in Buffer M (●) or in Buffer M + 1mM $MgCl_2$ + 35 μM AMPPNP (▲) (A) or at 1.75 μM MutL dimer loading concentration in Buffer M + 1 mM $MgCl_2$ with different [AMPPNP] **(B)**. The absorbance scans were collected at 280 nm or 230 nm **(A)** and at 292 nm **(B)** and analyzed using SEDFIT software to obtain c(s) distributions, which were integrated yielding $\bar{s}_{20,W}$. The smooth curve in **(B)** is a simulation using the best fit parameters derived from NLLS analysis of the isotherm to a model assuming two identical and independent binding sites for AMPPNP on a single MutL dimer (Eq. 5 in Material and Methods).

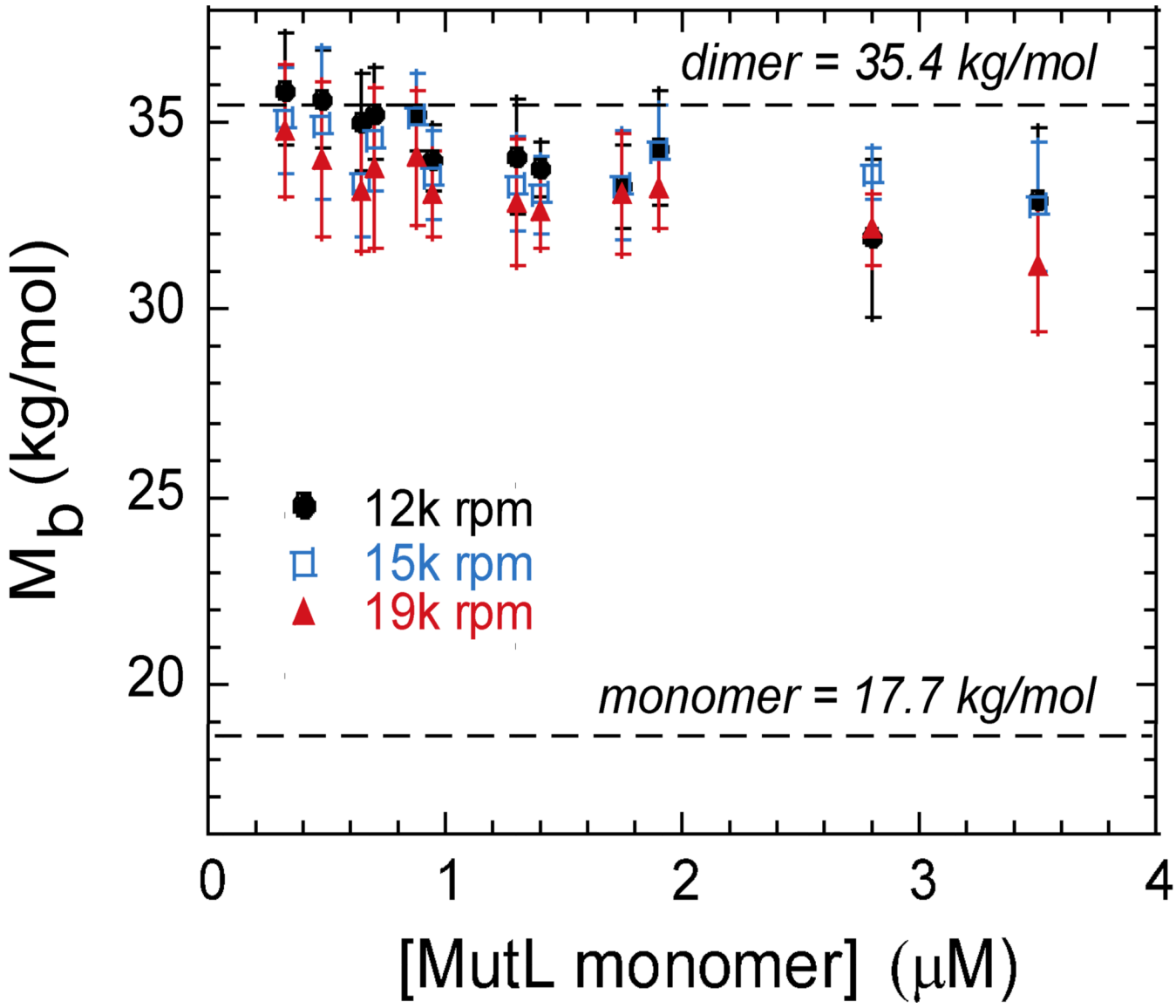

Figure 3.

Weight average buoyant molecular mass, $\bar{M}_b$, of MutL as a function of protein concentration. M_b was determined from sedimentation equilibrium experiments performed at 5°C for three rotor speeds (12,000, 15,000, 19,000 rpm) in Buffer M (50 mM potassium phosphate, pH 7.4 at 25°C, 50 mM KCl, 0.1 mM EDTA, 1 mM 2-mercaptoethanol). Each protein concentration distribution was fitted to a single ideal species model (n = 1 in Eq.1, Material and Methods). Values of M_b expected for MutL monomer and dimer are indicated by dotted lines and calculated assuming monomer M = 67923.95 g/mol and $\bar{\upsilon}_{5°C}$ = 0.7329 ml/g, based on amino acid sequence of MutL.

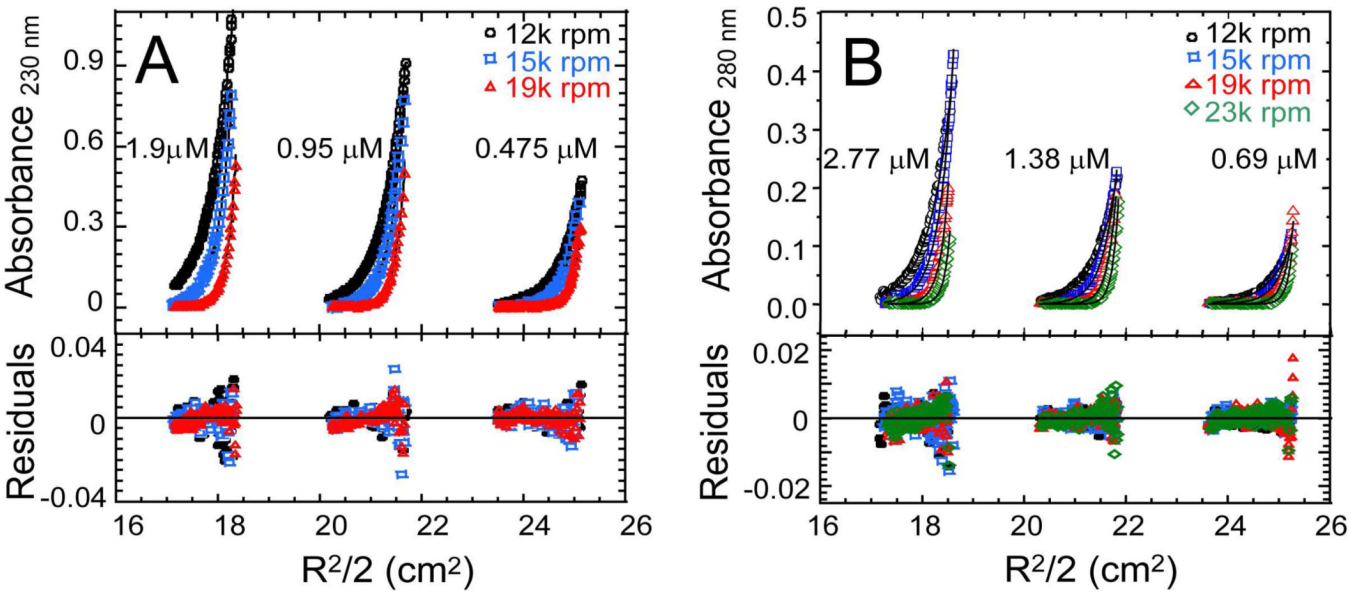

Figure 4.

Sedimentation equilibrium data indicates that MutL is a stable dimer. Experiments were performed for three different [MutL] indicated on the plot (total monomer loading concentration) at three or four rotor speeds (12,000 rpm, 15,000 rpm, 19,000 rpm and 23,000 rpm) at 5°C in Buffer M (**A**) or Buffer M +1mM $MgCl_2$ +35 μM AMPPNP (**B**). The smooth curves overlying the data are simulation using the best fit parameters resulting from global NLLS fit of all data sets to a single species model with residuals shown in the lower plot.

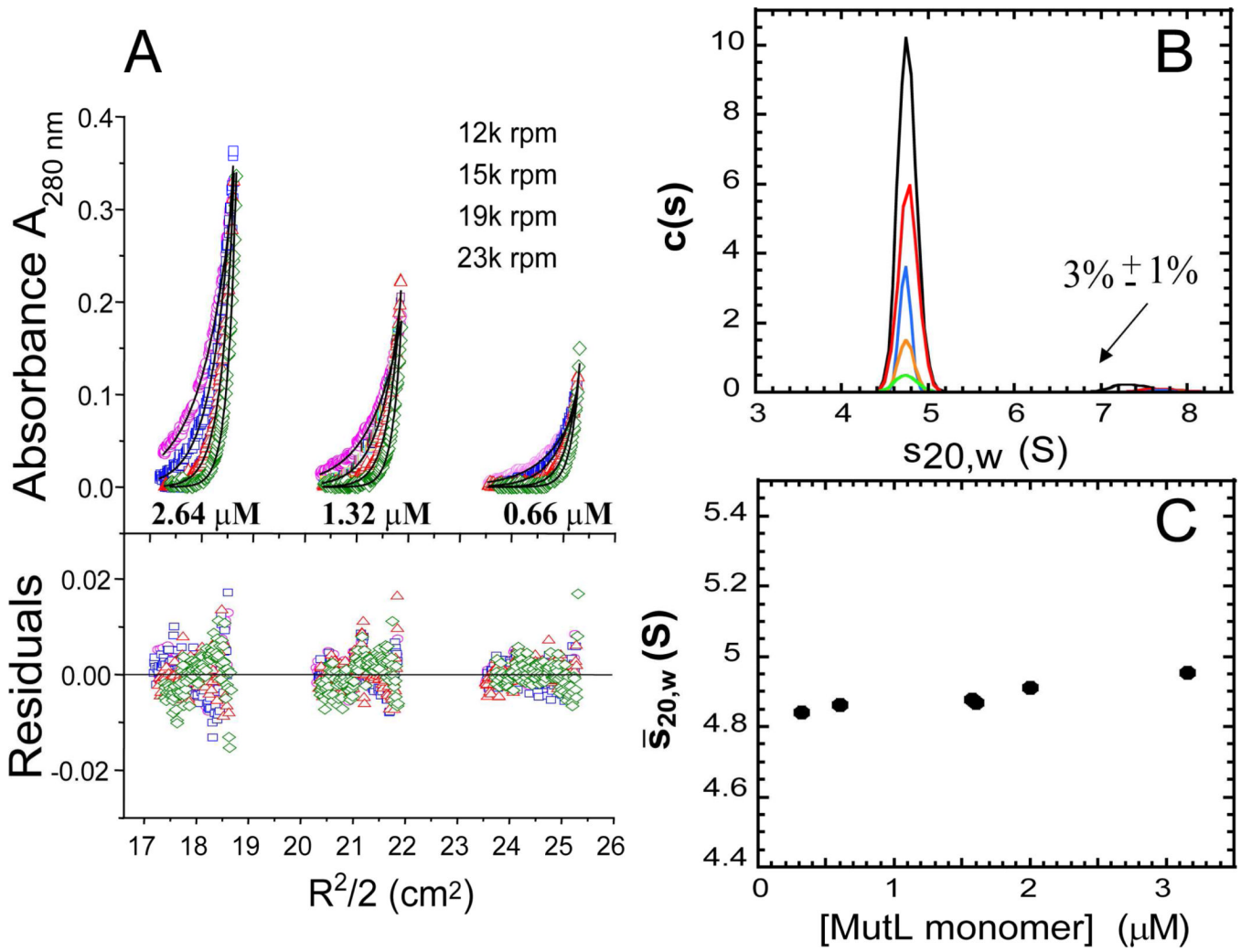

Figure 5.

MutL is a dimer in buffer M20/20. (**A**) Sedimentation equilibrium experiments were performed for three [MutL] (2.64, 1.32, 0.66 μM monomer) at four rotor speeds (12,000 rpm, 15,000 rpm, 19,000 rpm and 23,000 rpm) at 25°C in Buffer M20/20 (50 mM potassium phosphate, pH 7.4 at 25°C, 20 mM NaCl, 0.1 mM EDTA, 20 % glycerol, 1 mM 2-mercaptoethanol). The smooth curves overlying the absorbance data collected at 280 nm wavelength are simulation using the best fit parameters resulting from global NLLS fit of all data sets to a single species model with residuals shown in the plot below. (**B**). c(s) distribution for MutL (3.16, 2, 1.6, 0.6, 0.32 μM monomer) in buffer M20/20 at 25°C. The absorbance scans were analyzed using SEDFIT. (**C**) Weight average sedimentation coefficient, $\bar{s}_{20,w}$, as a function of [MutL] (μM monomer). Values of $\bar{s}_{20,w}$ were obtained by integration of c(s) curves.

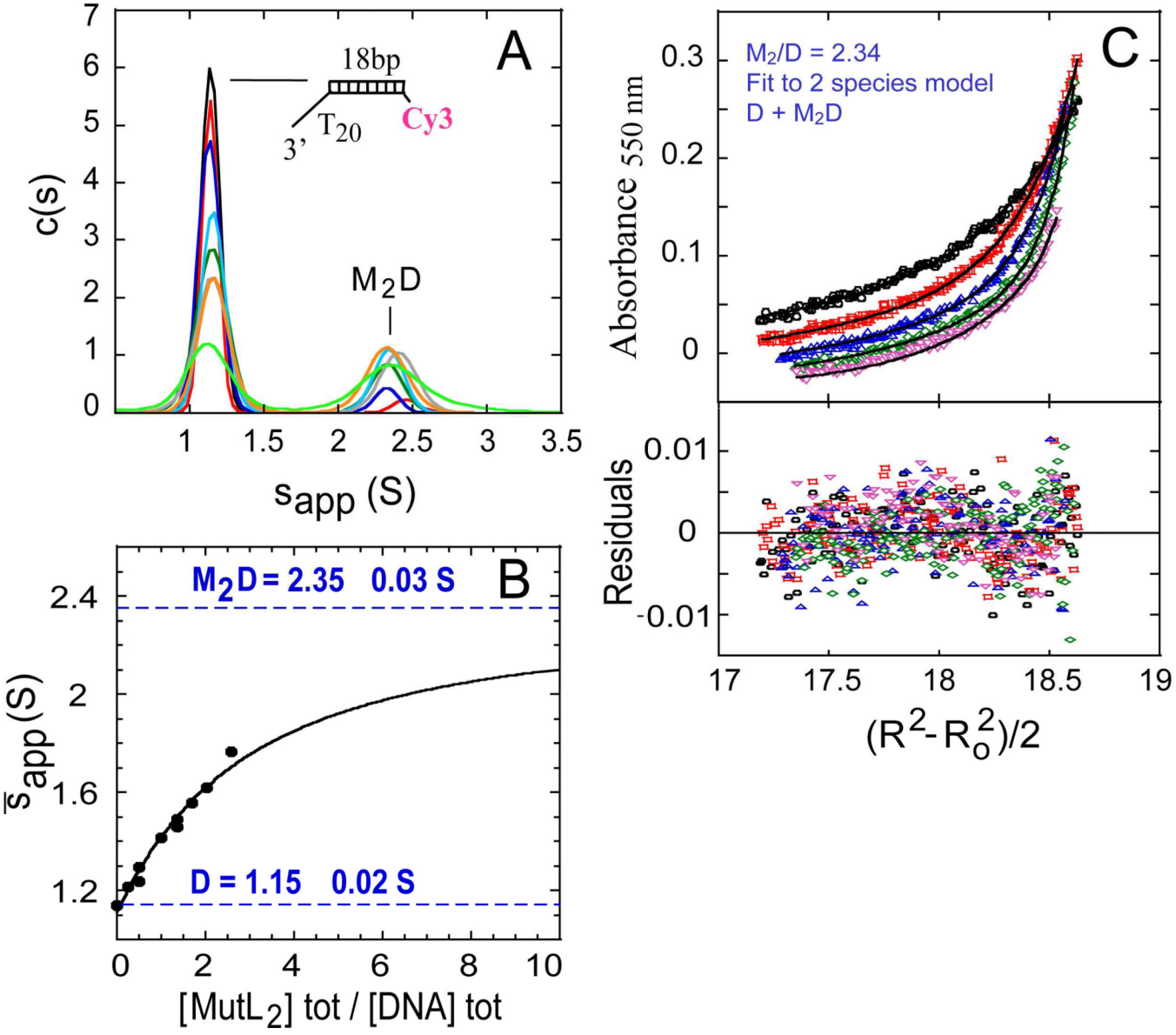

Figure 6.

Sedimentation velocity (**A, B**) and sedimentation equilibrium (**C**) study of the binding of MutL dimer (M_2) to a Cy3-labeled DNA unwinding substrate (a 3'(dT_{20})-ds18 DNA with Cy3 fluorophore attached to the 5' end of the bottom strand of the duplex, depicted schematically). Experiments were performed in buffer M20/20 at 25°C using total loading [Cy3-DNA] = 1.38 μM (**A**) or 1.2 μM (**C**). The absorbance profiles of Cy3 dye were monitored at 550 nm. (**A**) Sedimentation velocity experiments were performed at 42,000 rpm. Continues sedimentation coefficient distribution c(s) of Cy3-DNA in the presence of increasing [MutL dimer] (loading molar ratio of MutL dimer to DNA was: 0, 0.25, 0.5, 1, 1.37, 2, 2.59). Sedimentation coefficient are apparent, without correction to the standard conditions. Weight average sedimentation coefficient obtained by integration of area under the c(s) are depicted in (**B**) as a function of [MutL dimer] to [DNA] ratio. The smooth curve is a simulation using the best fit parameters derived from NLLS analysis of the data to a simple Langmuir isotherm (apparent binding constant of 34 (± 4.3) × 10_4 M^{-1}, Eq.6 in Material and Methods). (**C**) Cy3 absorbance profile for a representative sedimentation

equilibrium experiment carried out in 2.34 – fold molar excess of MutL dimer over Cy3-DNA at 12, 000; 15, 000; 18,000; 22,000 and 27,000 rpm). Data were analyzed by NLLS using a model that assumed presence of two sedimenting species in solution, one corresponding to the free Cy3-DNA and the other corresponding to DNA bound in complex with MutL dimer (n = 2 in Eq. 1, Material and Methods). The buoyant molecular mass of the free Cy3-DNA was fixed at value of 6.66 (± 0.22) kg mol^{-1} which was obtained experimentally in the same conditions. A best fit value of buoyant molecular mass of MutL-DNA complex equal to 39.605 ± 0.460 kg mol^{-1}, was obtained from NLLS analysis, which is in a reasonable agreement with a theoretical buoyant molecular mass of a single MutL dimer bound to Cy3-DNA molecule (35.56 kg mol^{-1}). Smooth curves overlaying the data are simulation using best fit parameters with residuals shown in the lower plot.

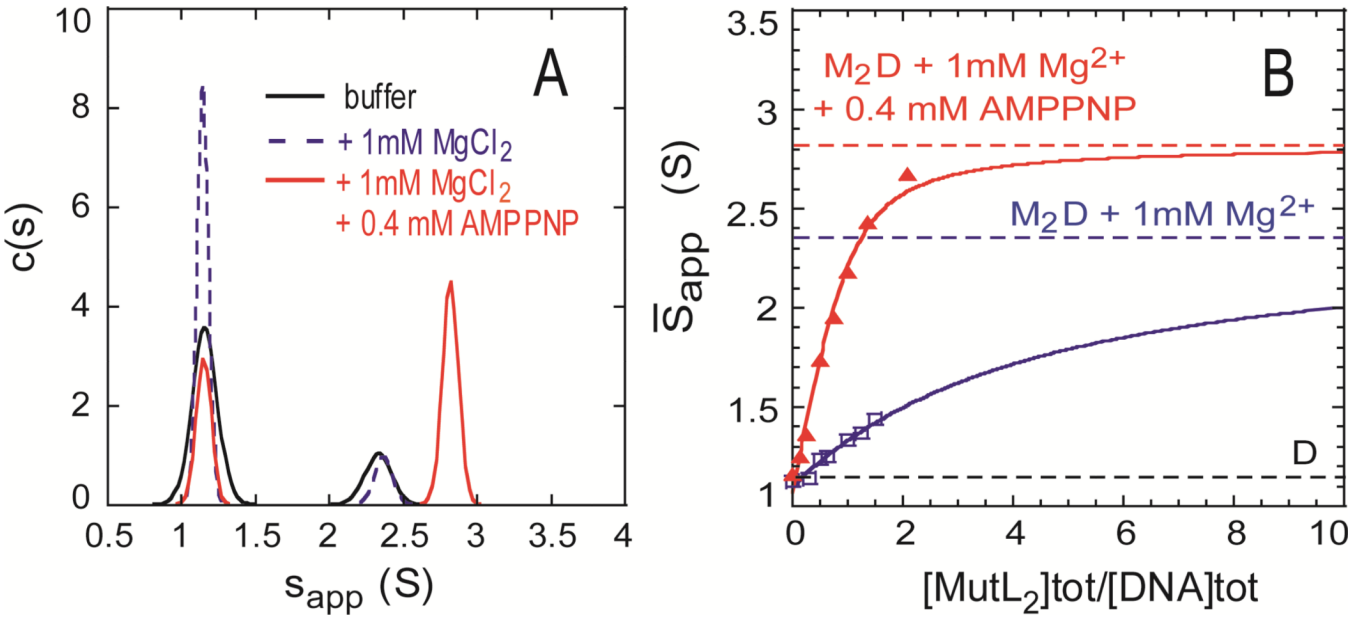

Figure 7.

Sedimentation velocity study of binding of MutL dimer to a 3'(dT_{20})-ds18 DNA. Experiments were performed at 25°C using total loading [Cy3-DNA] = 1.4 μM as a function of [MutL dimer] in buffer M20/20 (Buffer), in M20/20 + 1mM $MgCl_2$ (+ 1mM $MgCl_2$) or in M20/20 + 1mM $MgCl_2$ + 0.4 mM AMPPNP (+ 1mM $MgCl_2$ + 0.4 mM AMPPNP). The DNA concentration profiles were recorded by monitoring the absorbance of Cy3 dye at 550 nm. (**A**) Sedimentation velocity experiments were performed at 42,000 rpm. Representative c(s) distribution of Cy3-DNA in the presence of 1.4 μM of MutL dimer (molar ratio M_2/D = 1). Sedimentation coefficients are not corrected to the standard conditions. (**B**) Weight average sedimentation coefficient as a function of molar ratio of MutL dimer to DNA. The smooth curves are simulation using the best fit parameters derived from NLLS analysis of the data to a simple Langmuir isotherm and assuming that the plateau corresponds to the apparent s value for the MutL-DNA complex (+ $MgCl_2$: 2.36 ± 0.02 S, apparent binding constant of 19 (± 1.8) × 10^4 M^{-1}; + $MgCl_2$+AMPPNP: 2.82 ± 0.02 S, apparent binding constant of 38 (± 2.5) ×10^5 M^{-1} ; Eq. 6 in Material and Methods).

TABLE 1

Composition of Buffers	
Buffer	**Composition**
Buffer TGN 10/20/20	10 mM Tris (pH 8.3 at 25°C), 20% (v/v) glycerol, 20 mM NaCl, 1mM 2-mercaptoethanol
Buffer M	40.5 mM KH_2PO_4, 9.5 mM K_2HPO_4 (pH 7.4 at 25°C), 50 mM KCl, 0.1 mM EDTA, 1 mM 2-mercaptoethanol
Buffer M + Tris	10 mM Tris (with desired pH), 50 mM KCl, 0.1 mM EDTA, 1 mM 2-mercaptoethanol
Buffer M20/20	40.5 mM KH_2PO_4, 9.5 mM K_2HPO_4 (pH 7.4, 25°C), 20% (v/v) glycerol, 20 mM NaCl, 0.1 mM EDTA, 1 mM 2-mercaptoethanol,
Buffer N20/20	40.5 mM NaH_2PO_4, 9.5 mM Na_2HPO_4 (pH 7.4, 25°C), 20% (v/v) glycerol, 20 mM NaCl, 0.1 mM EDTA, 1 mM 2-mercaptoethanol,